Acta Chemica Scandinavica, 1994: 48: 37–45
Printed in Belgium – all rights reserved

ACTA
CHEMICA SCANDINAVICA
ISSN 0904-213X

Properties of $LaCo_{1-t}Cr_tO_3$. I. Solid Solubility, Thermal Expansion and Structural Transition

B. Gilbu, H. Fjellvåg and A. Kjekshus*

Department of Chemistry, University of Oslo, N-0315 Oslo, Norway

Gilbu, B., Fjellvåg, H. and Kjekshus, A., 1994. Properties of $LaCo_{1-t}Cr_tO_3$. I. Solid Solubility, Thermal Expansion and Structural Transition. – Acta Chem. Scand. 48: 37–45. © Acta Chemica Scandinavica 1994.

Samples of $LaCo_{1-t}Cr_tO_3$ were prepared with high compositional resolution for $0.00 \leqslant t \leqslant 1.00$, and were characterized by powder X-ray diffraction (PXD), differential scanning calorimetry (DSC) and infrared (FTIR) spectroscopy. $LaCo_{1-t}Cr_tO_3$ exhibits complete solid solubility. At room temperature the structure is distinctly rhombohedral for $t < 0.76$ and orthorhombic for $t > 0.84$. The extension of the implicit two-phase field within the thus established conversion region, $0.76 \leqslant t \leqslant 0.84$, could not be determined. In the investigated temperature range (120–1200 K) the transition from the low-temperature orthorhombic to high-temperature rhombohedral phase occurs for $t \geqslant 0.70$, the temperature of the transition increasing with increasing t. In the vicinity of the transition, the volume per formula unit is larger for the orthorhombic than for the rhombohedral phase. Thermal expansion coefficients decrease with increasing t, the change being subtle for $t \leqslant 0.60$ and more pronounced for $t > 0.60$. In IR spectroscopy the main feature is a shift of the absorption bands towards higher wavenumbers with increasing t up to $t = 0.60$, while the wavenumbers are more or less constant for $t \geqslant 0.75$. At $t \approx 0.60$ a splitting of certain IR bands also occurs. The parallel changes in properties considered in this study at $t \approx 0.60$ suggest that there may be a change in bonding characteristics around the stated value of the composition variable.

The current, considerable interest in oxides with perovskite-like structures stems to a large degree from their versatile use as catalysts, solid-state conductors and high-T_c superconducting materials. The ideal perovskite-type oxide, usually denoted ABO_3, contains a large cation, A, surrounded by 12 oxygen ions in a cubic close-packed array, and a smaller cation, B, situated in the octahedral interstices of the oxygen sub-lattice (Fig. 1a).

Catalytic studies have revealed that among the $LaTO_3$ (B = T = V, Cr, Mn, Fe, Co, Ni) perovskite-class oxides, $LaCoO_3$ is the one most active for CO oxidation.[1,2] So far, extensive studies of pure $LaCoO_3$ and A-site aliovalently substituted derivatives have been performed, while less work has been done to clarify effects introduced by B-site substitution.[3]

The present study forms an integral part of a program aimed at exploring the catalytic activity of the solid solution series $LaCo_{1-t}Cr_tO_3$ with regard to CO oxidation. As surface and catalytic properties are related to bulk properties, a thorough study of the physical properties of the solid solution system in question was performed prior to the catalytic testing.

In the following, a short overview of the physical properties of $LaCo_{1-t}Cr_tO_3$ is given. Attention is focused on generally accepted facts, while more uncertain points are considered in connection with relevant experimental data obtained in the present study.

The end members of the $LaCo_{1-t}Cr_tO_3$ solid solution series have slightly different crystal structures and differ in physical properties. $LaCoO_3$ takes rhombohedrally[4] (Fig. 1b) and $LaCrO_3$ orthorhombically[5] (Fig.1c) distorted perovskite-type structures at room temperature. $LaCrO_3$ undergoes a first-order phase transition to the rhombohedral arrangement at 533 K,[6,7] succeeded by a transition to the ideal cubic structure at 1920 K.[6,8] $LaCrO_3$ melts at 2500 K, and $LaCoO_3$ at 1740 K.[6]

$LaCoO_3$ is paramagnetic, but exhibits anomalous variations in the magnetic susceptibility at low temperatures[9] and in the temperature range 400–650 K.[10] The latter anomaly is reflected in the heat capacity of $LaCoO_3$[11] and appears to be accompanied by a gradual transformation from semiconducting to metallic behaviour.[12] The magnetic and electrical properties of $LaCrO_3$ are quite different from those of $LaCoO_3$. $LaCrO_3$ is a semiconducting[13,14] antiferromagnet, with a Néel temperature of 282 K.[15]

The whole composition range of $LaCo_{1-t}Cr_tO_3$ has in

* To whom correspondence should be addressed.

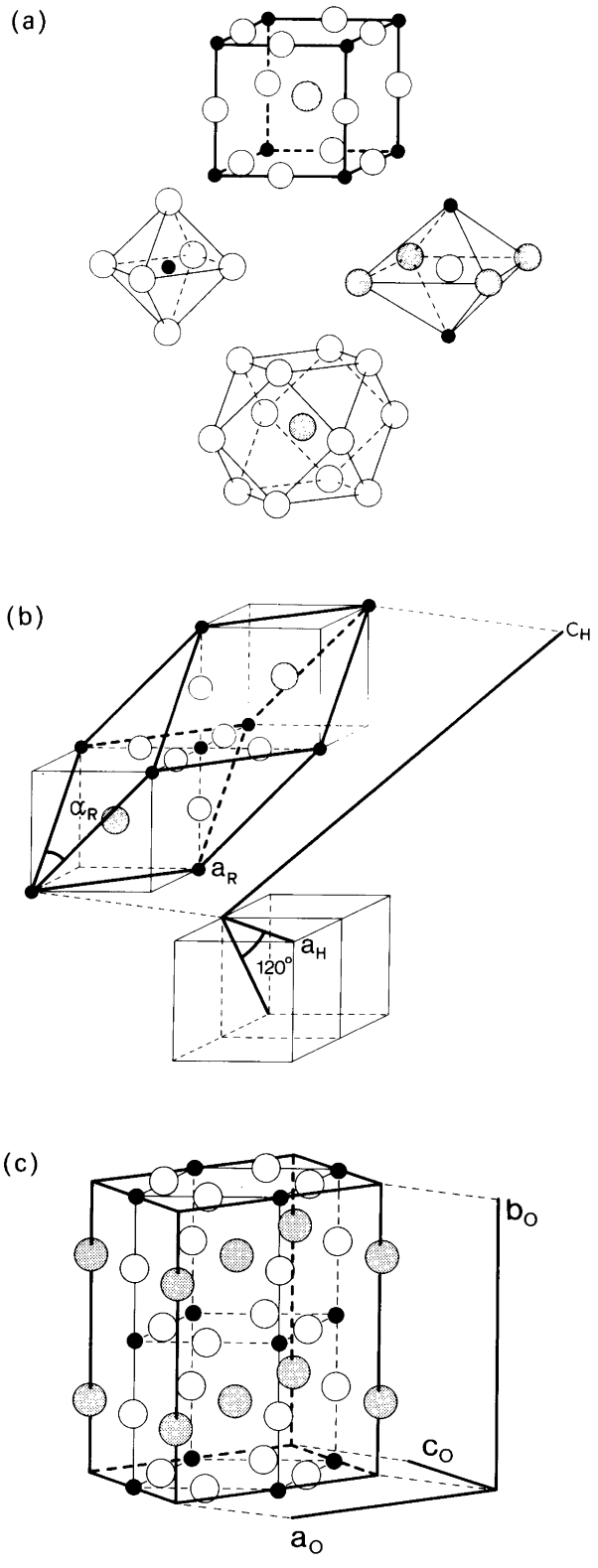

Fig. 1. Variants of the perovskite-type structure. (a) The prototype structure, emphasizing the octahedral coordinations of O (open circles) and B (here, B = T = Co/Cr; filled circles) and the twelve-coordination of A (here, A = La; shaded circles). (b) The rhombohedral variant, its hexagonal representation and their relation to the prototype structure. (c) The orthorhombic variant and its relation to the prototype structure.

principle been studied earlier with respect to structural, thermal and electrical properties by Tolochko *et al.*,[16,17] and with regard to sintering characteristics, thermal expansion and electrical properties by Sehlin *et al.*[18] and Koc *et al.*[19,20] All studies reported complete solid solubility. Tolochko *et al.*[16,17] found that the distortion of the perovskite-like atomic arrangement changes from rhombohedral to orthorhombic in the composition range $0.7 < t < 0.8$ at room temperature, and that the rhombohedral structure is favoured at higher temperatures. However, the studies of Tolochko *et al.*[16,17] are, for the present purpose, insufficient with respect to both compositional and temperature resolution. Tolochko *et al.*[16,17] established that the unit-cell volume per formula unit increases with t, but with rather small changes for $0.00 \leqslant t \leqslant 0.20$. The thermal expansion coefficient was found to decrease with increasing chromium content,[16,17,19] and for $t = 0.9$ and 1.0, contractions were observed around the orthorhombic to rhombohedral phase transition.[16,17]

The structural and physical properties of $LaCo_{1-t}Cr_tO_3$ at the temperatures employed in catalytic oxidation of CO are not yet well understood. The largest catalytic activity is established at temperatures where $LaCoO_3$ appears to undergo significant changes in the electric transport and magnetic properties. The changes in physical characteristics are in turn coupled to structural features (tilting of octahedra, unit cell volume, interatomic distances). The present contribution provides structural, thermal expansion and phase-transition data for the entire range of the $LaCo_{1-t}Cr_tO_3$ solid solution. Great care is taken to obtain a high degree of compositional resolution. In the succeeding papers in this series on $LaCo_{1-t}Cr_tO_3$, the crystallographic and magnetic ordering will be treated in part II, the magnetic and electronic properties in part III and the catalytic activity for CO oxidation in part IV.

Experimental

Samples of $LaCo_{1-t}Cr_tO_3$ were prepared with varying intervals in the different composition ranges. In the rhombohedral region, $0.00 \leqslant t \leqslant 0.70$, the interval was $\Delta t = 0.10$. In the region $0.76 \leqslant t \leqslant 0.85$, where the transition from rhombohedral to orthorhombic structure occurs around room temperature, a much narrower interval, $\Delta t = 0.01$, was selected, and in the orthorhombic region, $0.85 \leqslant t \leqslant 1.00$, $\Delta t = 0.05$ was used.

All samples were prepared by multiple firing of citrate gels. The starting materials were La_2O_3 (99.98%, Fluka), $Co(CH_3COO)_2 \cdot 4H_2O$ (>99.0%, Fluka), CrO_3 (>99%, Merck) and $C_3H_4(OH)(COOH)_3 \cdot H_2O$ (reagent grade, Sturge Biochemicals). Prior to use, La_2O_3 was heated to 1000°C to remove any hydrated and/or carbonated species. The actual metal contents of $Co(CH_3COO)_2 \cdot 4H_2O$ and CrO_3 were determined gravimetrically after heating the reactants to 750 and 800°C, respectively. The detected deviations from the

said formulae were compensated for during sample preparation.

In the first preparation step, citric acid was melted with La_2O_3. When most of the oxide was dissolved, the Co and/or Cr reagent(s) were added, along with water to obtain a volume two to four times that of the first step. When all constituents were dissolved, the citrate solution was placed in a furnace at 180°C, where it gradually lost water. During the dehydration, the citrate complexes formed a polymer gel with gradually increasing viscosity, which in turn lost more water and some carbon-containing species to form a porous, X-ray amorphous crust (xerogel). This porous solid was incinerated at 450°C to remove the major amount of carbonaceous species. At this stage, most samples were still X-ray amorphous, while some showed traces of microcrystalline phases, the latter being one or more of Co_3O_4, $LaCo_{1-t}Cr_tO_3$ and two yet unidentified compounds, which were probably oxide carbonates of La, Co and/or Cr. The samples were pressed into pellets and fired in air in three stages, first at 770°C for 20 h, then at 850°C for 30 h and finally at 850°C for 30 h. Between each heating stage, the samples were ground in a planetary mill. After the last firing, the samples were cooled slowly (1°C min^{-1}) to room temperature, with 10 h annealings at 700 and 500°C. This procedure is quite satisfactory with regard to product homogeneity. The complexation by citric acid assures homogeneity at the atomic level in the xerogel, and the firing–grinding procedure eliminates any inhomogeneities occurring after the combustion of the organic residues at 450°C. Later experiments have shown that it is sufficient to fire the samples twice at 800°C for 30 h, followed by slow cooling (1°C min^{-1}) to room temperature.

All samples were checked for purity and characterized by powder X-ray diffraction (PXD). Guinier–Hägg cameras were used, with Si ($a = 543.1065$ pm) as internal standard and $CrK\alpha_1$ ($\lambda = 228.970$ pm) radiation. The detection limits of possible La_2O_3 and Co_3O_4 impurities in a $LaCoO_3$ product were determined through extrapolation of the intensities for the strongest La_2O_3 and Co_3O_4 reflections for mechanically mixed standard samples. The PXD photographs were measured by a Nicolet L18 film scanner, controlled by the program SCANPI.[21] Both detection limits were about 0.3 wt%. All results reported in this series refer to samples which were phase-pure within the detection limits for the said oxides.

High-temperature PXD was performed at temperatures between 290 and 1200 K using a Guinier–Simon camera (Enraf–Nonius) and $CuK\alpha_1$ ($\lambda = 154.0598$ pm) radiation. The samples were placed in open quartz capillaries and heated at a rate of 30 K h^{-1}. The same instrument was used for low-temperature PXD between 123 and 420 K, with a cooling rate of 14 K h^{-1}. The phase transitions were studied under conditions of both increasing and decreasing temperature for three samples ($t = 0.80$, 0.90 and 1.00, at rates of 25 or 45 K h^{-1}).

Position and intensity measurements of all PXD films were performed manually, using a comparator. Unit-cell parameters at all temperatures were derived by least-squares calculations using the CELLKANT program.[22]

DSC was performed, using a Mettler TA 3000 system. The powder samples were placed in aluminium containers, with holes pierced in their lids to allow equilibrium with air at all times. The heating rate for all samples was 10 K min^{-1}.

FTIR spectroscopy in the region 4000–350 cm^{-1} was performed on a Bruker IFS 88 spectrometer, connected to an Aspect 1000 computer. Specimens of 1 wt% $LaCo_{1-t}Cr_tO_3$ in KBr tablets were used.

Results and discussion

Colour. All samples were obtained as powders, and the colour (see also Fig. 2) as seen by the naked eye ranges from black for $LaCoO_3$, via brown for $LaCo_{0.25}Cr_{0.75}O_3$ to light green for $LaCrO_3$. When viewed with a light microscope, the samples appear greenish gray with a metallic lustre in the range $0.00 \leqslant t \leqslant 0.70$. With a further increase in t, the colour looks less metallic and more orange. At $t = 0.95$ the samples are yellow, and for $LaCrO_3$ the colour is light green, as is characteristic for the d–d transitions associated with Cr^{3+}.

Unit-cell dimensions and phase conversion as functions of composition. The compositional variation in the unit-cell

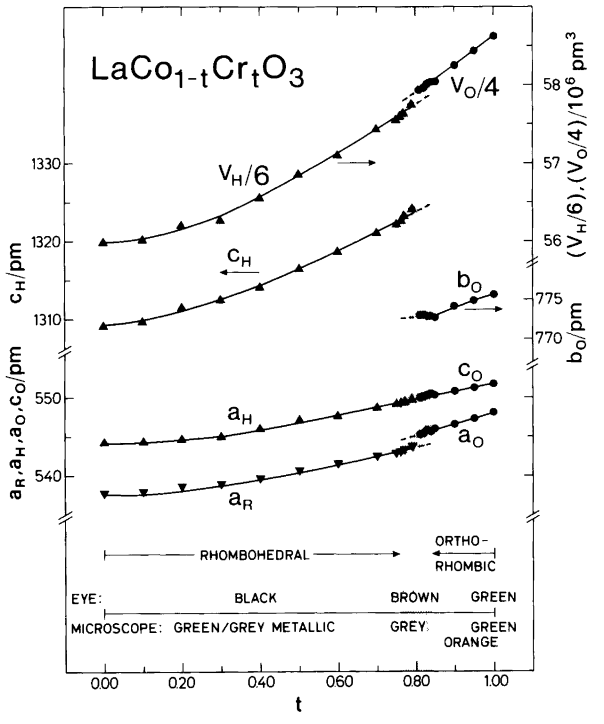

Fig. 2. Unit-cell dimensions of $LaCo_{1-t}Cr_tO_3$ for $0.00 \leqslant t \leqslant 1.00$. Calculated errors do not exceed the size of symbols. Triangles and circles refer to the rhombohedral (R) and orthorhombic (O) regions, respectively. The variation in sample colour with t, as seen both by the naked eye and through an optical microscope with reflected light, is indicated at the bottom of the illustration.

dimensions of the rhombohedral (R) and orthorhombic (O) solid-solution phases at room temperature is shown in Fig. 2. The rhombohedral unit cell is specified in the hexagonal setting (marked with index H) and the orthorhombic in the standard setting *Pnma*, even though *Pbnm* was applied in the previous structure determination.[5] The unit-cell dimensions for the end members are in accord with those found in Refs. 4 and 5. The present results differ from those of Tolochko *et al.*,[16,17] but since the accuracy of the present unit-cell data is judged to be considerably better, no further attention will be given to these earlier findings.

At room temperature $LaCo_{1-t}Cr_tO_3$ takes the rhombohedral structure variant in Fig. 1b for $t < 0.76$ and the orthorhombic variant in Fig. 1c for $t > 0.84$. Samples with composition $0.76 \leqslant t \leqslant 0.84$ show PXD reflections characteristic of both variants. For each sample in the conversion range, the unit-cell dimensions (Fig. 2 and *vide infra*) were calculated assuming the coexistence of the O and R phases. In each case the structure type resulting in the lowest standard deviations according to the CELLKANT[22] computations was chosen as the majority phase. The calculations for $t = 0.78$ and 0.80 gave extraordinarily high standard deviations, and these data were hence omitted from Fig. 2, even though the results were in accord with the results for the other samples.

The unit-cell volume increases non-linearly with increasing chromium content in the entire solid-solution range. For all samples, the unit-cell volume is less than expected for ideal mixing, indicating positive interactions between the Co and Cr atoms. From Fig. 2 it is seen that a discontinuous increase in the unit-cell volume occurs when the atomic arrangement changes from rhombohedral to orthorhombic.

To envisage the structural conversion, one may start by observing the relations of the orthorhombic and rhombohedral variants to the ideal cubic (C) perovskite-type structure (Fig. 1a). In the rhombohedral variant (Fig. 1b), with the volume relationships $V_R = 2V_C$ and $V_H = 6V_C$, the structure is contracted along one body diagonal. Thus, three of the four threefold symmetry axes are eliminated, while the fourth is maintained and corresponds to c_H. The compression along the body diagonal deforms the originally square faces of the 'basic cube' to rhombs. The two face diagonals now differ, the longest corresponding to a_H, the shortest to a_R. In the orthorhombic arrangement (Fig. 1c), with $V_O = 4V_C$, the 'basic cube' is doubled and compressed along b_O as well as compressed along one face diagonal in the cubic *ac*-plane, the two resulting face diagonals corresponding to a_O and c_O. A further comparison of the O and R variants shows that a_O and c_O correspond to a_R and a_H, respectively. When the structure changes from R to O with increasing t, one face diagonal, a_H, is constant, while the other, a_R, increases and approaches a_H (Fig. 2). Thus the deformation of the 'rhombohedral $a_R a_H$ plane' is diminished, and the increase in a_R (which corresponds to a_O) yields the observed increase in the volume per formula unit (Fig. 2).

In a discussion of phase transitions, symmetry must also be taken into account. As pointed out by Geller,[23] the symmetry constraints imply that the transition between the rhombohedral and orthorhombic structures must be of first order. Geller's reasoning is based on the space group $R\bar{3}m$ for $LaCoO_3$, whereas the actual space group is $R\bar{3}c$. This, however, does not invalidate the conclusion, since *Pnma* (pertinent to the orthorhombic variant) is not a subgroup of either.

A first-order phase transition in a solid-solution phase implies the existence of a two-phase region, both in terms of composition and temperature. However, owing to large standard deviations in the unit-cell dimensions of the minority phase, a region of constant unit-cell parameters could not be verified, and no conclusive evidence regarding the extent of the inferred two-phase region was found. Furthermore, it was attempted to detect the two-phase region more directly by following the evolution of the *d*-values for appropriate reflections. No consistent pattern was found, as some reflections showed a constant *d*-value in one composition region, others in another region, while yet other reflections unveiled a continuous variation with increasing t. In fact, visual inspection of the PXD diagrams, with regard also to reflection intensities, even suggested that the transition is gradual.

However, in evaluating these findings, one must bear in mind that on increasing t, the first reflection unequivocally indexable on the orthorhombic unit cell occurs at $t = 0.76$, and the last which must be indexed rhom-

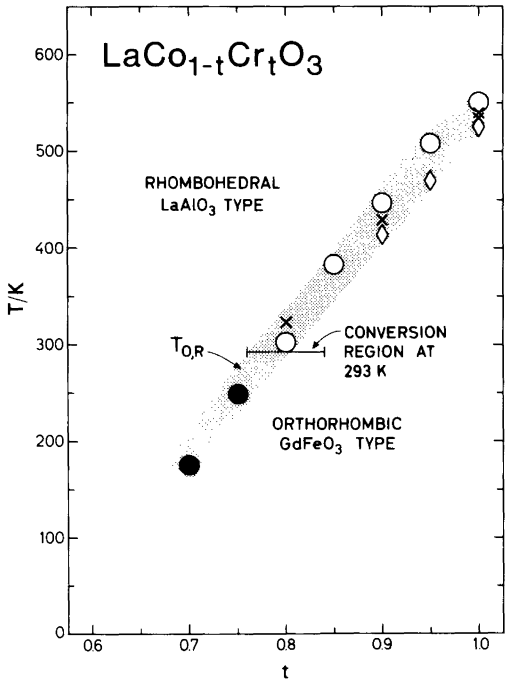

Fig. 3. Structural phase diagram for $LaCo_{1-t}Cr_tO_3$. Orthorhombic to rhombohedral transition temperatures marked ○ were determined by PXD with increasing temperature, ● by PXD with decreasing temperature and ◇ by DSC with increasing temperature; X refers to data from Refs. 6, 7 and 17. Shading covers the thermal hysteresis region.

bohedrally disappears at $t = 0.84$. Regardless of the seemingly continuous variation in unit-cell dimensions within this composition range, these compositions define the maximum extent of the inferred two-phase region.

Phase transition as function of temperature. All samples which take the orthorhombic arrangement at room temperature undergo a phase transition to the rhombohedral structure at elevated temperatures, and as seen from Fig. 3, the temperature of the transition, $T_{O,R}$, increases with increasing Cr content. PXD showed that samples in the composition range $0.70 \leqslant t \leqslant 0.76$ transformed to the orthorhombic structure upon cooling below room temperature. In view of the nearly linear, rather rapid decrease of the transition temperature for $0.70 \leqslant t \leqslant 1.00$ (Fig. 3), which extrapolates to $T_{O,R} = 0$ K for $t = 0.55$, and the 123 K lower temperature limit for the PXD equipment, samples with $t < 0.70$ were not studied with regard to $T_{O,R}$.

$T_{O,R}$ was extracted from the high- or low-temperature PXD as the lowest temperature where reflections from the rhombohedral phase are found in runs with increasing temperature and as the highest temperature where the orthorhombic phase is detected in decreasing temperature runs. Within the uncertainty of the measurements (10 K), no definite two-phase region could be detected as a func-

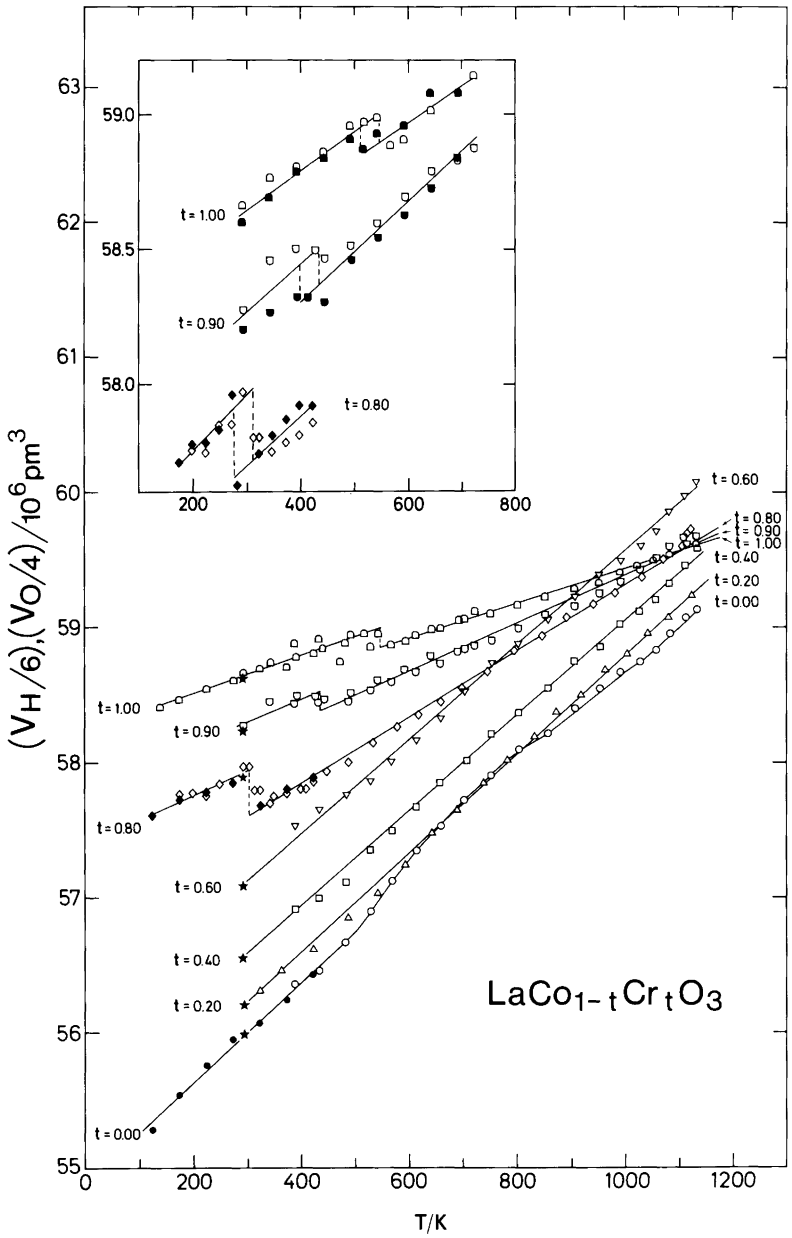

Fig. 4. Compositional evolution of the volume thermal expansion characteristics for $LaCo_{1-t}Cr_tO_3$. Inset shows hysteresis loops for $t = 0.80$, 0.90 and 1.00. Open and closed symbols refer to increasing and decreasing temperature conditions, respectively.

tion of temperature for any of the samples which undergo the O to R transition. This is in accord with the findings regarding the structural conversion as a function of composition.

The phase transition for samples with composition $t = 0.80$, 0.90 and 1.00 was studied upon both increasing and decreasing temperature. The unit-cell volume per formula unit versus temperature characteristics are shown in the inset to Fig. 4. The thermal hysteresis of the phase transition is 33 ± 8 K, irrespective of composition and heating rate (25 and 45 K h^{-1}). The volume contraction upon the transition to the rhombohedral structure is [0.25(7), 0.13(7) and 0.10(5)] $\times 10^6$ pm^3 per formula unit for $t = 0.80$, 0.90 and 1.00, respectively. The unit-cell volume per formula unit is thus distinctly smaller for the rhombohedral than for the orthorhombic variant in the vicinity of the phase transition. This is both qualitatively and quantitatively consistent with the volume change found as a function of composition at room temperature. For compositions around $t = 0.80$, the volume change per formula unit at room temperature is estimated from Fig. 2 to be $0.15(4) \times 10^6$ pm, whereas that obtained as function of temperature (inset to Fig. 4) amounts to $0.25(7) \times 10^6$ pm^3.

The O to R transition is also observed by the DSC technique. In these measurements, the transition is evident as an endothermal effect on increasing temperature. The heat of transition increases gradually with increasing chromium content, the effect being barely observable at $t = 0.80$ and 0.85, at which compositions the peak is too diffuse to allow a reasonably accurate estimate of the transition temperature. DSC measurements were also performed by Tolochko *et al.*[17] to determine $T_{O,R}$. Their results are in general accord with the present ones, even though their reported transition temperatures refer to the peak values from the DSC curves, while the onset temperatures are presently employed. An intriguing point is that Tolochko *et al.* report a sizeable DSC peak for $t = 0.80$, as opposed to the indistinct peaks which were observed for the samples of $t = 0.85$ and 0.80 presently examined. The O to R transition temperatures as established by DSC are juxtaposed to those found by PXD in Fig. 3, where results reported in Refs. 6, 7 and 17 are included for comparison. The shading covers the observed thermal hysteresis region.

Thermal expansion. The thermal expansion of selected samples throughout the entire solid-solution range was determined from high- and low-temperature PXD. Because no internal standard was used in these measurements, the calculated values of the unit-cell dimensions were adjusted to conform with the room-temperature values. To facilitate comparison between the orthorhombic and rhombohedral phases, the volumes in Fig. 4 are presented per formula unit.

For $LaCoO_3$, the expansion curves for both the volume and the individual axes (in the hexagonal setting) take an extended sigmoidal shape (Figs. 4 and 5). Alternatively,

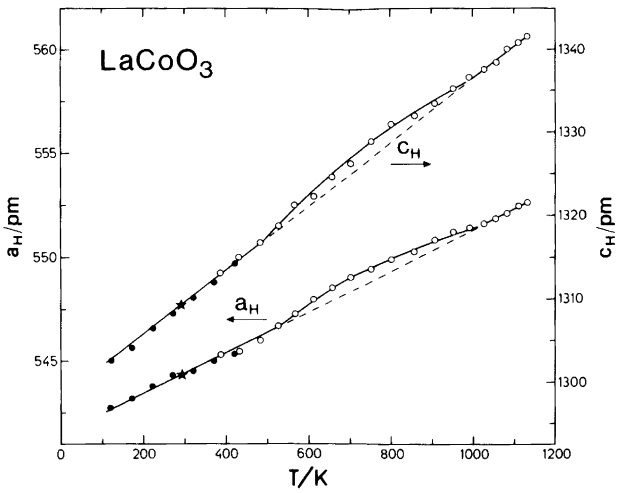

Fig. 5. Temperature dependence of a_H and c_H for $LaCoO_3$. Open and closed symbols refer to increasing and decreasing temperature conditions, respectively.

the curves may be described as composed of two linear regions with nearly equal slopes, separated by a non-linear region. The largest thermal expansion coefficient occurs in the non-linear region, and in roughly the same temperature range, DSC shows a broad endothermal effect (Fig. 6).

For the compositions $t = 0.20$, 0.40 and 0.60, the deviation from linearity in the thermal expansion characteristics is small through the entire temperature range studied. The sample with $t = 0.20$ exhibits an indistinct endothermal effect (in DSC) in a temperature region where there seems to be a deviation from linearity in the volume expansion behaviour. However, since the possible non-linearity is of the same order as the uncertainty in the experimental points, the expansion curves for $t = 0.20$, 0.40 and 0.60 were approximated as linear. For the compositions $t = 0.80$, 0.85, 0.90, 0.95 and 1.00, the expansion curves are composed of two straight lines, one for the orthorhombic and one for the rhombohedral phase (Fig. 4; for clarity, the thermal expansion curves for $t = 0.85$ and 0.95 are omitted from the illustration).

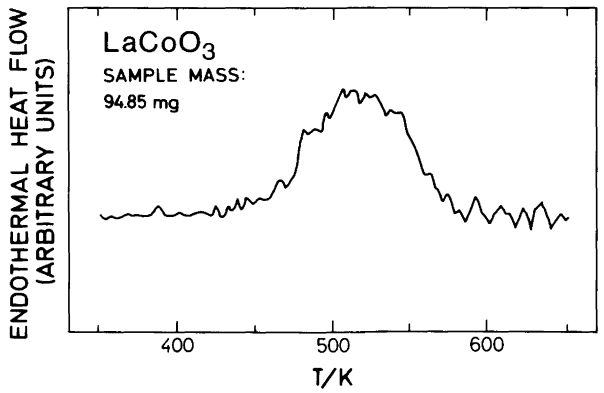

Fig. 6. Raw curve from DSC scan for $LaCoO_3$ fitted on a temperature-independent baseline, showing the endothermal heat flow versus temperature.

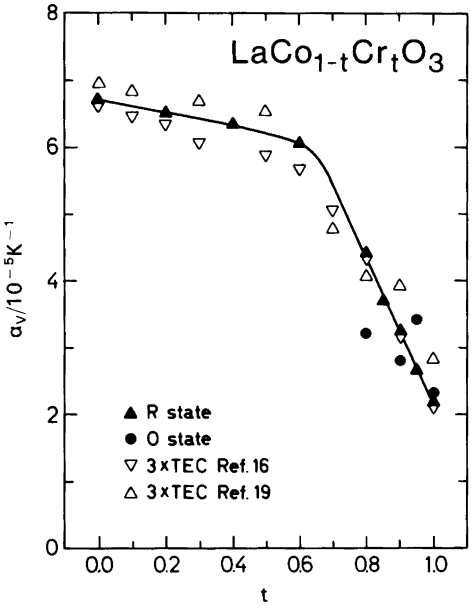

Fig. 7. Variation in the linear volume thermal expansion coefficient, α_V, with t for $LaCo_{1-t}Cr_tO_3$. See Table 1 for information on the temperature ranges where the marked α_V apply.

The thermal expansion coefficients (α_x) were established from the gradients of the linear approximations to the expansion curves and are expressed as $\alpha_x = (1/x_T) \times (\Delta x/\Delta T)$, with $x = a$, b, c or V and using $T = 293$ K whenever relevant. For the rhombohedral region, the linear approximation must be characterized as good, whereas larger uncertainties are encountered in the orthorhombic region. The latter feature is in part a reflection of fewer data points in the orthorhombic region. In both structural regions an acceptable agreement was found between the axial and volume thermal expansion coefficients.

A plot of α_V versus t is shown in Fig. 7. α_V is large and decreases only slightly for $0.00 \leqslant t \leqslant 0.60$, followed by a significant reduction in value for $0.60 < t < 1.00$. From Table 1, it is seen that α_{a_H} is more or less constant while α_{c_H} gradually decreases for $t \leqslant 0.60$, whereas both coefficients decrease significantly for $t > 0.60$. The present thermal expansion data are in reasonable accord with the linear thermal expansion coefficients (TEC) found dilatometrically by Koc and Anderson[19] and Tolochko *et al.*[16] (Fig. 7). Their numerical values were multiplied by three to obtain volume thermal expansion coefficients. The present expansion coefficients for $LaCo_{1-t}Cr_tO_3$ are considered to be the most accurate, since the previous reports refer to sintered multicrystalline rods, where additional uncertainty, due to both preferred crystallite orientation and a considerable volume fraction of macroscopic voids, is introduced. It should also be noted that α_{a_H}, α_{c_H} and α_V for the R state of $LaCrO_3$ from the data of Geller and Raccah[7] are significantly larger than the values in Table 1. Owing *inter alia* to the internal consistency of the large amount of data presently obtained and the frequent temperature calibrations (against an Ag standard) of our instrument, the current results are considered to be more correct.

Table 1. Thermal expansion coefficients in $10^{-5}\,K^{-1}$ for $LaCo_{1-t}Cr_tO_3$. Numerals in italics refer to the orthorhombic phase. Last digit is uncertain.

t	Temperature range/K	α_a	α_b	α_c	α_V
0.00	100–500[a]	1.81		2.96	6.70
0.20	290–1200	1.82		2.74	6.49
0.40	380–1140	1.82		2.58	6.33
0.60	380–1140	1.69		2.54	6.03
0.80	*100–300*	*1.6*	*1.3*	*0.5*	*3.2*
0.80	300–1140	1.17		2.04	4.42
0.85	380–1140	0.971		1.72	3.70
0.90	*290–450*	*0.4*	*1.2*	*0.95*	*2.8*
0.90	450–1140	0.806		1.59	3.23
0.95	*380–490*	*0.92*	*0.24*	*1.4*	*3.4*
0.95	520–1140	0.621		1.40	2.66
1.00	*100–520*	*0.76*	*0.57*	*0.98*	*2.3*
1.00	530–1140	0.466			2.19

[a] and 1000–1140.

IR spectroscopy. IR spectra for $LaCo_{1-t}Cr_tO_3$ showed a gradually increasing transmission in the region 4000–900 cm^{-1}. In this spectral region, no distinct absorption bands were found. IR spectra in the region 900–350 cm^{-1} for samples of composition $t = 0.00$, 0.20, 0.40, 0.60, 0.80 and 1.00 are shown in Fig. 8. The varia-

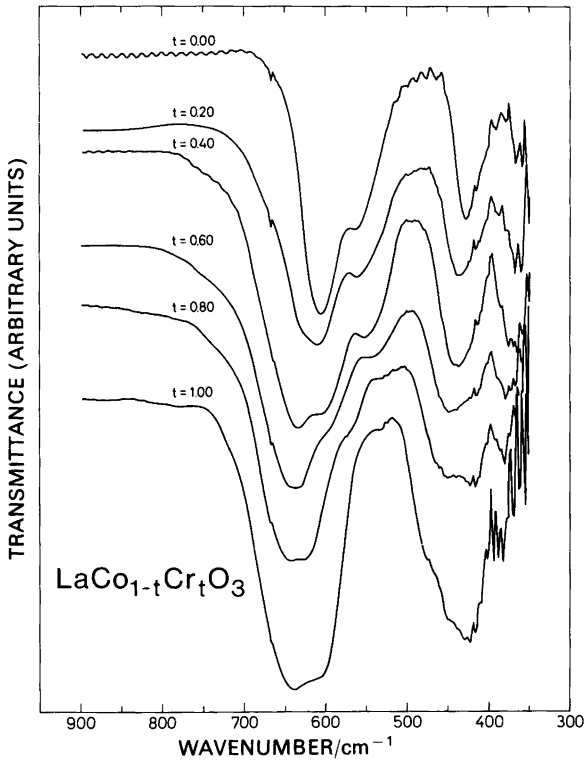

Fig. 8. IR spectra of $LaCo_{1-t}Cr_tO_3$ with $t = 0.00$, 0.20, 0.40, 0.60, 0.80 and 1.00.

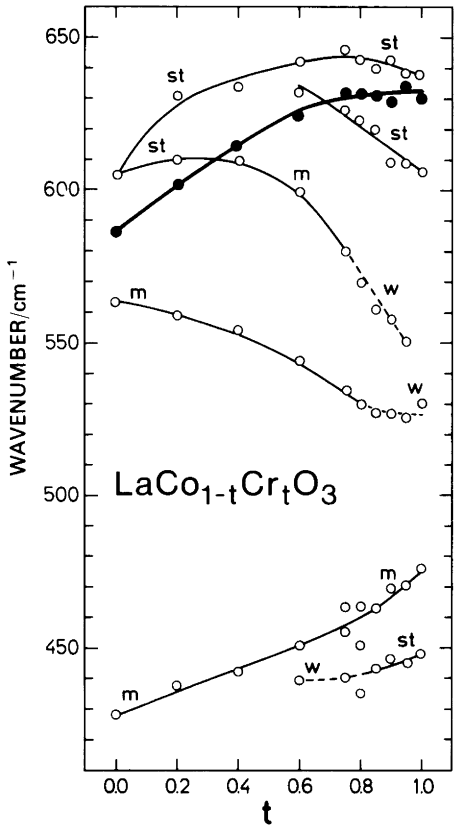

Fig. 9. Compositional variation for the centre of gravity of the composite IR band (●) for $LaCo_{1-t}Cr_tO_3$ at about 600 cm^{-1} and of individual bands (○) at wavenumber greater than 420 cm^{-1}. Estimated uncertainty in wavenumber is ± 5 cm^{-1}.

tion in wavenumber for distinguishable, intense peaks as a function of composition is presented in Fig. 9. The prominent features of the spectra are the composite absorption bands at some 600 and 450 cm^{-1}. The former band probably corresponds to a stretching of the metal–oxygen bond and the latter may correspond to a bending of the oxygen–metal–oxygen bonds within the $(Co/Cr)O_6$ octahedra.[24] Another composite band at about 380 cm^{-1} may also be attributed to the bending of bonds within these octahedra. The present IR findings are in general accord with earlier reports[24,25] for $LaCoO_3$ and $LaCrO_3$.

A major feature in the development of the IR spectra with increasing t is the shift in the centre of gravity of the metal–oxygen stretching peak from 585 cm^{-1} for $t = 0.00$ to 630 cm^{-1} for $t = 1.00$. For $0.00 \leqslant t \leqslant 0.60$ the change in wavenumber is fairly rapid, while the value is more or less constant for $0.75 \leqslant t \leqslant 1.00$ (Fig. 9). Such a shift towards higher wavenumber might be attributed both to decreasing mass and increasing bond strength as Co is substituted by Cr. The oxygen–metal–oxygen bending modes at about 450 cm^{-1} also exhibit an increase in wavenumber with increasing chromium content (Fig. 9). Visual inspection of the spectra suggests that the same development applies to the composite band in the vicinity of 380 cm^{-1}.

Another interesting point is the apparent splitting of both the stretching and bending absorption bands at around $t = 0.60$. Although a detailed analysis of these features requires data over and above those presently available, the phenomenon may qualitatively be interpreted as follows: Incorporation of Cr in $LaCoO_3$ diminishes the local symmetry of the lattice, thus giving rise to additional IR-active bands, as well as modifying existing bands. Because Cr is statistically distributed through the lattice, the bulk symmetry as seen by PXD is not affected. The intensity of the Cr-induced bands will depend on the Cr^{3+} ion concentration in the lattice, and because the wavenumbers of these bands are not very different from those of the modified $LaCoO_3$ bands, the Co- and Cr-induced bands do not separate until there is a large concentration of Cr^{3+} ions in the lattice. Subsequently, it is also observed that certain bands are weakened and even disappear as t approaches unity.

It is of interest to compare the compositional development of the IR spectra to that of the thermal expansion coefficient, as both characteristics reflect lattice vibrations. Although quantitative comparisons are not possible, it should be noted that there is a qualitative change in the compositional variation of both properties at a composition around $t = 0.60$.

Acknowledgment. This work has received financial support from the Norwegian Council for Science and the Humanities (NAVF).

References

1. Wachowski, L. *Z. Phys. Chem. 269* (1988) 743.
2. Tascón, J. M. D. and Tejuca, L. G. *React. Kinet. Catal. Lett. 15* (1980) 185.
3. Yamazoe, N. and Teraoka, Y. *Catal. Today 8* (1990) 175.
4. Thornton, G., Tofield, B. C. and Hewat, A. W. *J. Solid State Chem. 61* (1986) 301.
5. Khattak, C. P. and Cox, D. E. *Mat. Res. Bull. 12* (1977) 463.
6. Coutres, J.-P., Badie, J. M., Berjoan, R., Coutures, J., Flamand, R. and Rouanet, A. *High Temp. Sci. 13* (1980) 331.
7. Geller, S. and Raccah, P. M. *Phys. Rev. B 4* (1970) 1167.
8. Traverse, J.-P. and Berjoan, R. *C. R. Acad. Sci., Ser. C 276* (1973) 1167.
9. Menyuk, N., Dwight, K. and Raccah, P. M. *J. Phys. Chem. Solids 28* (1967) 549.
10. Raccah, P. M. and Goodenough, J. B. *Phys. Rev. 155* (1967) 932.
11. Horinouchi, K., Takahashi, Y. and Fueki, K. *Yogyo Kyokaishi 89* (1981) 104.
12. Thornton, G., Morrison, F. C., Partington, S., Tofield, B. C. and Williams, D. E. *J. Phys. C 21* (1988) 2871.
13. Subba Rao, G. V., Wanklyn, B. M. and Rao, C. N. R. *J. Phys. Chem. Solids 32* (1971) 345.
14. Tripathi, A. K. and Lal, H. B. *J. Mater. Sci. 17* (1982) 1595.
15. Bertaut, E. F., Mareschal, J., de Vries, G., Aléonard, R., Pauthenet, R., Rebouillat, J. P. and Zarubicka, V. *IEEE Trans. Magn. 2* (1966) 453.
16. Tolochko, S. P., Kononyuk, I. F., Zonov, Yu. G. and

Ivashkevich, L. S. *Izv. Akad. Nauk SSSR, Neorg. Mater. 23* (1987) 829. [Eng. transl. *Inorg. Mater. 23* (1988) 743.]
17. Tolochko, S. P., Kononyuk, I. F., Lyutsko, V. A. and Zonov, Yu. G. *Izv. Akad. Nauk SSSR, Neorg. Mater. 23* (1987) 1520. [Eng. transl. *Inorg. Mater. 23* (1988) 1342.]
18. Sehlin, S., Anderson, H. U., Koc, R. and Sparlin, D. M. *Ceram. Trans. 24* (1991) 249.
19. Koc, R. and Anderson, H. U. *J. Mater. Sci. Lett. 11* (1992) 1191.
20. Koc, R. and Anderson, H. U. *J. Eur. Ceram. Soc. 9* (1992) 285.
21. Werner, P. E. *Program SCANPI, Version 6*, Institute of Inorganic Chemistry, University of Stockholm, Sweden 1988.
22. Ersson, N. O. *Program CELLKANT*, Chemical Institute, University of Uppsala, Sweden 1981.
23. Geller, S. *Acta Crystallogr. 10* (1957) 243.
24. Subba Rao, G. V., Rao, C. N. R. and Ferraro, J. R. *Appl. Spectrosc. 24* (1970) 436.
25. Ganguly, P. and Vasanthacharya, N. Y. *J. Solid State Chem. 61* (1986) 164.

Received May 23, 1993.